Model-Based Real-Time Control for Laser Induced Thermal Therapy with Applications to Prostate Cancer Treatment

Yusheng Feng[a], David Fuentes[b], R. Jason Stafford[b], and J. Tinsley Oden[c]

[a]Computational Bioengineering and Nanotechnology Lab, The University of Texas at San Antonio, San Antonio, TX 78749, USA
[b]Department of Imaging Physics, University of Texas M.D. Anderson Cancer Center, Houston, TX 77030, USA
[c]Institute for Computational Engineering and Sciences, The University of Texas at Austin, Austin, TX 78712, USA

ABSTRACT

In this paper, we present a model-based predictive control system that is capable of capturing physical and biological variations of laser-tissue interaction as well as heterogeneity in real-time during laser induced thermal therapy (LITT). Using a three-dimensional predictive bioheat transfer model, which is built based on regular magnetic resonance imaging (MRI) anatomic scan and driven by imaging data produced by real-time magnetic resonance temperature imaging (MRTI), the computational system provides a regirous real-time predictive control during surgical operation process. The unique feature of the this system is its ability for predictive control based on validated model with high precision in real-time, which is made possible by implementation of efficient parallel algorithms. The major components of the current computational systems involves real-time finite element solution of the bioheat transfer induced by laser-tissue interaction, solution module of real-time calibration problem, optimal laser source control, goal-oriented error estimation applied to the bioheat transfer equation, and state-of-the-art imaging process module to characterize the heterogeneous biological domain. The system was tested *in vivo* in a canine animal model in which an interstitial laser probe was placed in the prostate region and the desired treatment outcome in terms of ablation temperature and damage zone were achieved. Using the guidance of the predictive model driven by real-time MRTI data while applying the optimized laser heat source has the potential to provide unprecedented control over the treatment outcome for laser ablation.

Keywords: Laser-tissue interaction, MRI and MRTI, image-guided therapy, laser induced thermal therapy, modeling and simulation, predictive real-time control, bioheat transfer, model validation, parallel computing

1. INTRODUCTION

Laser induced thermal therapy (LITT), in particular, laser-induced interstitial thermal therapy, can be modulated to deliver thermal energy to specific tumor regions with very sharp precision, which is a preferable minimally invasive thermal therapeutic modality for soft-tissue diseases. The magnetic resonance temperature imaging (MRTI) technique, which has medical merits in its own right, is used as the guidance to provide precise control of the laser source based on accurate model prediction and achieve the desired treatment outcome.[5] The model-based real-time control system was successfully tested with K9 animal experiments and has potential to be translated into a thermal therapy for human.

In this paper, we present a computational system capable of pre-treatment planning and real-time predictive control based on optimization with respect to selected quantities of interest (temperature, cell/tissue damage or other biomakers). Using both magnetic resonance imaging (MRI) and magnetic resonance thermal imaging (MRTI) data, we are able to construct predictive three-dimensional computer models that are calibrated and validated with MRTI measurement streaming feedback imaging data every five seconds. These imaging data are then used as input for model-based predictive control. There are fundamental challenging issues need to

Further author information: (Send correspondence to Y.F.)
Y.F.: E-mail: yusheng.feng@utsa.edu, Telephone: 1 210 458 6479

Optical Interactions with Tissue and Cells XX, edited by Steven L. Jacques, E. Duco Jansen, William P. Roach,
Proc. of SPIE Vol. 7175, 717515 · © 2009 SPIE · CCC code: 1605-7422/09/$18 · doi: 10.1117/12.816875

be addressed in order to construct such a model-based real-time control system with the acceptable precision and reliability. These issues include: (1) medical Imaging and data processing, (2) mathematical modeling of laser-tissue interaction, (3) bioheat transfer in tissue and cellular response, (3) mesh generation and numerical simulation, (4) cell damage and tissue characterization, (5) inverse problem and efficient parallel computing, (6) treatment planning and outcome prediction, (7) real-time surgical monitoring and control, and (8) model validation with *in vitro* and *in vivo* experimentation. This paper aims to provide an overview of the current status and capabilities of the computational system to the problems of model calibration, optimization of laser source and real-time control for laser induced thermal therapy. We demonstrate, based on canine *in vivo* animal experiments, that our predictive computational model of bioheat transfer that employs real-time, patient specific data can provide high fidelity control during the laser treatment process. At the core of this computational system are the main components of an adaptive *hp*-finite element approximation to the nonlinear parabolic Pennes equation and solution process of adjoint-based algorithms for inverse analysis, model calibration, and adaptive control of cell damage.

The significance of this work is not only that the real-time optimal control of surgical protocol can be achieved during surgery but also that the prediction of treatment outcomes are based on biologically relevant quantities that characterize effectiveness of the treatment outcome. In this paper, we present the second generation of the computational system that is more efficient in terms of implementation and parallel execution. Another unique feature of this second generation system is that the spatial dependency of thermal properties of tissues (i.e., tissue heterogeneity) can be taken into account explicitly and updated in real-time.

2. IMAGE-GUIDED LASER THERAPY

The physical basis for thermal therapies, such as LITT, is that exposing cells to the elevated temperature for certain period of time will result in irreversible damage and even destroying the cells. The primary goal of minimally invasive ablative thermal therapies is to deliver a lethal dose to the target tissue while sparing normal tissue. Therefore, the effectiveness of any thermal therapy, including cryotherapy, microwave, radio-frequency, ultrasound, or laser therapy, relies on the precise control of the energy deposition to the targeted region. Using advanced modeling and simulation methods, it is possible to provide predictive control based on real-time aquisition of temperature imaing data.

Current MR imaging technology can easily produce anatomical images of internal organs includig tumor detection. However, it will be more useful if these images overlaid with temperature field using MRTI (MR Temperature Imaging) technology in thermal therapy. MRTI has the the ability to provide fast, quantitative temperature imaging in a variety of tissues, and this information can be combined with biological models of damage in order to estimate the extent of injury following the therapy.[1] In addition, real-time image guidance with high resolution[2,3] has the potential to facilitate unprecedented control over any thermal therapies provided that the bioheat transfer model is predictive, i.e., efficient to be executed before the thermal energy takes effect on tissues. In the early work, we has been demonstrated with the first generation of the computational framework capable of inducing precise temperatures.[4,5] We note that the computational framework presented here is quite general and can be used for other image-guided therapy.

During the laser surgical experiments, the temperature distribution was measured by *in vivo* MRTI with the proton-resonance frequency-shift method. All experiments were performed at the University of Texas M.D. Anderson Cancer Center in Houston, Texas, on a 1.5-T MR scanner (Excite HD, GEHT, Waukesha, WI) equipped with high-performance gradients (23 mT/m maximum amplitude and 120 T m^{-1} sec^{-1} maximum slew rate) and fast receiver hardware (bandwidth, ±500 MHz). T_1- and T_2-weighted images were used to plan and localize the treatment by verifying the position of the laser fiber relative to the imaged region prior to irradiation. MRTI was performed by using a complex phase-difference technique with a fast, two-dimensional RF-spoiled gradient-recalled echo sequence (TR/TE = 49.5 ms/20 ms, flip angle = 30°, bandwidth = 9.62 kHz). To achieve a five-second per image scan rate with a field of view 240×240 mm^2 The change in temperature from baseline after a number of images was extrapolated from the complex-valued MRTI data by using the temperature dependence of the proton resonance frequency shift and a temperature sensitivity with coefficient of -0.0097 ppm/°C. The temperature resolution for MRTI measured temperature difference is less than 1°C.

3. BIOHEAT TRANSFER AND LASER-TISSUE INTERACTION

In this section, we discuss the modeling process for laser induced thermal response. When laser light is applied to the biological tissues, various interaction mechanisms can be initiated based on the power density and exposure time. It is a commonly belief that [8] there are five major types of interactions may occur: plasm-incuded ablation, photodisruption, photoablation, thermal interaction, and photochemical interaction. Another interaction may involve photomechanical phenomena in this temperature range. In the most of cases of medical application, however, the laser tissue interaction mainly falls into thermal interaction regime.

There is a rich body of literature resulting from the investigation of the thermal process of laser interacting with biological tissues .[6–9] The tissue parameters for charactering the laser tissue interaction are coefficients of reflection, absorption, and scattering. Together they determine the total transmission of the tissue at certain wavelength. The thermal properties are the heat conductivity and heat capacity. On the other hand, the laser radiation parameters include wavelength, exposure time, focal spot location, and power density and energy level.

The effect of thermal interaction induced by laser can be modeled by a bioheat transfer equation.[10] We generalize the traditional Pennes equation to take into account of nonlinearity for temperature dependency and heterogeneity for spatial variation. The mathematical representation of the temperature distribution in the tissue incorporates both the Pennes bioheat equation for the thermal effects of local blood perfusion and an expression for laser energy as a thermal source. Both tissue and laser properties can take local value to account for heterogeneity.

Let Ω be a bounded domain (tumor region) in $\mathcal{R}^3$ with $\Gamma = \partial\Omega_{\mathrm{C}} \bigcup \partial\Omega_{\mathrm{N}}$ denoting a Lipschitz continuous boundary. Furthermore, let Ω_m be sub-region of Ω, i.e.

$$\Omega_m \subset \Omega, \quad m = 1, 2, \cdots, M \quad \text{and} \quad \overline{\left\{ \bigcup_{m=1}^{M} \Omega_m \right\}} = \Omega \bigcup \partial\Omega_{\mathrm{C}} \bigcup \partial\Omega_{\mathrm{N}}$$

The following equation is the generalized version of Pennes bioheat equation with temperature (nonlinear) and spatially dependent (non-homogenous) coefficients.

$$\rho c_p \frac{\partial T}{\partial t} - \nabla \cdot (k(\mathbf{x}, T)\nabla T) + \omega(\mathbf{x}, T) c_b (T - T_a) = Q(\mathbf{x}, t) \qquad \text{in } \Omega_m \tag{1}$$

The thermal conductivity, k $[J\, s^{-1} m^{-1} K^{-1}]$, and blood perfusivity, ω $[kg\ s^{-1}\ m^{-3}]$, are assumed to be bounded functions of the temperature field, $T = T(\mathbf{x}, t)$, where

$$k(\mathbf{x}, T) = k_\circ(\mathbf{x}) + k_1(\mathbf{x})\ \mathrm{atan}(k_2(\mathbf{x})(T - k_3(\mathbf{x}))) \qquad \omega(\mathbf{x}, T) = \omega_\circ(\mathbf{x}) + \omega_1(\mathbf{x})\ \mathrm{atan}(\omega_2(\mathbf{x})(T - \omega_3(\mathbf{x})))$$

and $k_\circ(\mathbf{x})[Js^{-1}m^{-1}K^{-1}]$, $k_1(\mathbf{x})[Js^{-1}m^{-1}K^{-1}]$, $k_2(\mathbf{x})[K^{-1}]$, $k_3(\mathbf{x})[K]$, $\omega_\circ(\mathbf{x})[kg\ s^{-1}\ m^{-3}]$, $\omega_1(\mathbf{x})[kg\ s^{-1}\ m^{-3}]$, $\omega_2(\mathbf{x})[K^{-1}]$, and $\omega_3(\mathbf{x})[K]$ are spatially dependent parameters of the diffusivity and perfusivity coefficient functions defined above. In other words, we permit localized thermal parameters to account for spatial heterogeneity. The specific heat of the tissue and blood are given by c_p and c_b respectively, T_a is the arterial temperature, and ρ is the density of the tissue. On the Cauchy boundary,

$$-k(\mathbf{x}, T)\nabla T \cdot \mathbf{n} = h(T - T_\infty) \qquad \text{on } \partial\Omega_{\mathrm{C}} \text{ and } \mathbf{x} \in \Omega_m$$

The coefficient of cooling is denoted h. T_∞ denotes the ambient temperature. $\mathcal{G}$ is the prescribed heat flux on the Neumann boundary.

$$-k(\mathbf{x}, T)\nabla T \cdot \mathbf{n} = \mathcal{G} \qquad \text{on } \partial\Omega_{\mathrm{N}} \text{ and } \mathbf{x} \in \Omega_m$$

The temperature field is propagated forward in time from a given initial condition, $T_\circ$.

$$T(\mathbf{x}, 0) = T_\circ \qquad \text{in } \Omega_m$$

The heating provided by a laser source is commonly modeled based on transport theory and characterized by the absorbed heat that can be represented by the rate of heat generation $Q(\mathbf{x}, t)$ that is defined as

$$Q(\mathbf{x}, t) = \mu_a \, \Phi(\mathbf{x}, t) = \mu_a \mu_{tr} P(t) \frac{3 \exp(-\mu_{eff} \|\mathbf{x} - \mathbf{x}_\circ\|)}{4\pi \|\mathbf{x} - \mathbf{x}_\circ\|}, \quad \mathbf{x} \in \Omega_m \tag{2}$$

where $\mu_{tr} = \mu_a + \mu_s(1-g), \qquad \mu_{eff} = \sqrt{3\mu_a \mu_{tr}}$

and $\Phi(\mathbf{x}, t)$ is the fluence that defines the amount of energy, in the form of photons, passing through a unit area at a point in space per unit time. $P(t)$ is the laser power at time t. The parameters μ_a, μ_s are absorption and scattering coefficients that relate to laser wavelength. They can be considered as the probability of absorption and scattering, respectively, of photons in tissues. The constant g is the anisotropic factor, and $\mathbf{x}_\circ$ is the position of the laser source. It is important to note that all the optical properties can also be considered as a spatially dependent functions to account for heterogeneity. We have designed very efficient parallel algorithms so that the solution can be evaluated in real-time. Of course, the laser tissue interaction can also be modeled directly using the Monte Carlo method. However, this approach will prohibit real-time prediction.

4. THERMAL DAMAGE BASED OPTIMIZATION

Although temperature is an obvious choice for optimal control, it however cannot be used as the quantity in the objective function.[11] Since the goal of the laser therapy is to eradicate tumor while preserving the surrounding health tissues, more biological relevant quantities of interest should be used for optimization. For optimal treatment outcome, we choose thermal damage as the measure for the effectiveness of LITT. For cancer recurrence, we may select biomarkers such as the level of heat shock proteins as an indicator.[12]

Thermal damage processes in cells and tissues are very complex in which various pathological transformations such as DNA damage, cell necrosis, or coagulation in tissue may occur. One way to quantify thermal damage is to use the *cell damage index* Ω defined as

$$\Omega = \ln\left(\frac{C(T,0)}{C(t,T)}\right) \tag{3}$$

When cell viability function $C(t,T)$ is normalized and $C(T,0)$ is set to one, we have $\Omega = -\ln C(t,T)$. For the purpose of optimization, we need to transform Ω, which has the range of $[0, \infty)$, to F_d that has a finite range $[0, 1]$ by defining $F_d = 1 - e^{-\Omega}$.

Now, the question is how to characterize cell viability $C(t,T)$ under the various thermal conditions. In the commonly used Arrhenius model, an assumption is made that the rate of cell damage is proportional to the rate of reaction $k(T) = Ae^{-\frac{E_a}{RT}}$, where E_a is the activation energy (or the heat of activation), R is the universal gas constant, and T is the absolute temperature (ref.[13] for a review of thermal damage models). The cell viability function is, therefore,

$$C(t,T) = C_0 e^{A\,t\,e^{-E_a/RT(t)}} \tag{4}$$

which is a double exponential form. For normalized cell viability function, $C_0 = 1$. Thus, the cell damage index based on the traditional Arrhenius model is

$$\Omega = \int_0^\tau A e^{\frac{-E_a}{RT(t)}} \, dt \tag{5}$$

where τ is the total exposure time and A a constant that is often referred as to the frequency factor.

Although thermal damage models based on the traditional Arrhenius law are widely used due to its simplicity, the model possesses two major inherent limitations: (1) its inability to fit all the cellular damage data over the entire thermotherapeutic temperature range and throughout the entire heating process, and (2) its sensitivity to small changes in parameters due to its double exponential function form. It is reported that the frequency factor A ranges from $O(10^5)$ to $O(10^{218})$.[14] Of course, these frequency factors correspond to different cell-lines.

However, this phenomenon is most likely due to the numerical sensitivity resulting from double exponential form for cell viability.

One alternative is to use the two-state model,[15] which is derived based on statistical thermodynamics, to fit the cell viability data in a wider temperature range (for other alternatives, we refer to a review article by He and Bischof[13]). Based on the basic principal of thermodynamics, a cell population with two distinctive state (live and dead) can be described by $C(\tau, T)$ denoting the cell viability function and $D(\tau, T)$ denoting the cell damage function, which have the following forms

$$C(\tau,T) = \frac{e^{-G(\tau,T)/kT}}{1+e^{-G(\tau,T)/kT}}, \quad D(\tau,T) = \frac{1}{1+e^{-G(\tau,T)/kT}} \tag{6}$$

where T, t and k are temperature, the exposure time and Bolzman constant, respectively. Here, $G(\tau, T)$ is of the form $H - TS$, where H is a constant and $S(\tau)$ is a linear function $S = \alpha_o t + \beta_o$, and $h = H/k$, $\alpha = \alpha_o/k$, and $\beta = \beta_o/k$ are constants. The quantities G, H, and S have the same dimensions as Gibbs free energy, enthalpy, and entropy, respectively. Thus, these quantities can be referred as activation free energy, activation enthalpy, and activation entropy. Moreover, the cell damage index can be directly calculated by Eqn.(3) without integration.

5. CALIBRATION AND REAL-TIME PREDICTIVE CONTROL

The generalized nonlinear heterogeneous Pennes model, Eqn. (1), has been shown to provide very accurate prediction of bioheat transfer and is used as the basis of the finite element prediction. The model-based predictive control involves the solution process of three major problems: calibration of the generalized Pennes bioheat transfer model to patient specific MRTI data, optimal positioning and power supply of the laser heat source, and computing goal oriented error estimates. During the laser treatment process, all three problems are solved in tandem by separate groups of processors communicating amongst each other as needed. The variational form of the governing Pennes bioheat transfer model is as follows:

Given a set of model, β, and laser, η, parameters,
Find $u(\mathbf{x}, t) \in \mathcal{V} \equiv H^1\left([0,T], H^1(\Omega)\right)$ s.t.
$$B(u, \beta; v) = F(\eta; v) \qquad \forall v \in \mathcal{V}$$

where the explicit functional dependence on the model parameters, β, and laser parameters, $\eta = (P(t), \mathbf{x}_0)$, are expressed as follows

$$B(u,\beta;v) = \int_0^T \int_\Omega \left[\rho c_p \frac{\partial u}{\partial t} v + k(u,\beta)\nabla u \cdot \nabla v + \omega(u,\beta) c_{blood}(u - u_a)\, v\right] dxdt + \int_0^T \int_{\partial\Omega_C} hu\, v\, dAdt + \int_\Omega u(\mathbf{x},0)\, v(\mathbf{x},0)\, dx$$

$$F(\eta;v) = \int_0^T \int_\Omega 3P(t)\mu_a\mu_{tr} \frac{\exp(-\mu_{eff}\|\mathbf{x}-\mathbf{x}_0\|)}{4\pi\|\mathbf{x}-\mathbf{x}_0\|} v\, dxdt + \int_0^T \int_{\partial\Omega_C} hu_\infty\, v\, dAdt - \int_0^T \int_{\partial\Omega_N} \mathcal{G}\, v\, dAdt + \int_\Omega u^0\, v(\mathbf{x},0)\, dx$$

$$\mu_{tr} = \mu_a + \mu_s(1-\gamma) \qquad \mu_{eff} = \sqrt{3\mu_a\mu_{tr}}$$

Here $k\left[\frac{J}{s\cdot m\cdot K}\right]$ and $\omega\left[\frac{kg}{s\ m^3}\right]$ are bounded functions of u, c_p and c_{blood} are the specific heats, u_a the arterial temperature, ρ is the density, and h is the coefficient of cooling. P is the laser power, μ_a, μ_s are laser coefficients related to laser wavelength and give probability of absorption of photons by tissue, γ is the anisotropy factor, and $\mathbf{x}_0$ is the position of laser photon source. Constitutive model data and details of the optimization process are given in.[5,12]

To simulate laser surgery and make reliable predictions of the temperature field requires two major modeling components: a bioheat transfer model for the tissue and a laser source term that characterizes thermal energy deposited into the tissue.

Here, we use a nested-optimization algorithm, introduced in,[16] to solve the calibration problem based on the generalized Pennes bioheat transfer model, Eqn. (1). The goal is to capture dynamic changes in tissue properties due to biological alteration as well as nanoshell inclusion. In order to achieve this goal, the objective function, Eqn. (7), for the calibration problem is defined as the difference in space-time norm between the computed temperature field, $T(\mathbf{x}, t)$, and the temperature field obtained from the MRTI experiments, $T_{exp}(\mathbf{x}, t)$, integrated over the entire biological domain Ω and time duration of interest $[0, \tau]$. The computed temperature field $T(\mathbf{x}, t)$ is an implicit function of the bioheat transfer model parameters β, a vector that consists of the location of the laser probe, absorption and scattering coefficients, and parameters in conductivity and perfusion functions.

The main question to be addressed is how to approximate the full optimization problem efficiently so that the prediction can be made prior to the next data arrival. In other words, the speed of computation needs to be faster than the rate of data acquisition, at least fast enough to make necessary adjustment based on the model prediction during the time of the operation. The optimization problem can be formally stated as:

Find β^* such that $\mathcal{F}(\mathcal{T}(\beta), \beta)$ is minimized, where

$$\mathcal{F}(T(\beta), \beta) = \frac{1}{2} \int_0^{\tau} \int_{\Omega} (T(\beta)(\mathbf{x}, t) - T_{exp}(\mathbf{x}, t))^2 \, dxdt \tag{7}$$

In order to speed up solution time for the approximation, Eqn. (7) is replaced by a sequence of smaller problems with less historical data in the time dimension.

Find β_i^* such that $\mathcal{F}_i(T(\beta), \beta)$ is minimized, where

$$\mathcal{F}_i(T(\beta_i), \beta_i) = \frac{1}{2} \int_0^{\tau_i < \tau} \int_{\Omega} (T(\beta_i)(\mathbf{x}, t) - T_{exp}(\mathbf{x}, t))^2 \, dxdt \tag{8}$$

using a smaller time window $[0, \tau_i] \subset [0, \tau_{i+1}] \subset [0, \tau], i = 1, 2, 3, \cdots$. The nested-block optimization process carries the solution process from Calibration $\rightarrow$ Prediction $\rightarrow$ Validation/Calibration $\rightarrow$ Prediction, as *in vivo* MRTI measurement data being imported into the model every five seconds.

Based on the experiment, the temperature field is calibrated with respect to MRTI thermal images of heating of a mouse tumor treated with nanoshells. A nonlinear form of Pennes bioheat transfer model, Eqn. (1), is calibrated to predict the heat transfer in tissues. There is a trade-off between accuracy and efficiency. An efficient optimization process will allow faster solution time for the calibration so that it can be used in real-time surgical control. However, time constraints of real-time computation do not permit the computation of the Hessian of the objective function, which would allow a more accurate measure of rate change with respect to each model parameter as a solution is approached. Thus, we compute the gradient of the objective function using a limited-memory variable metric by a quasi-Newton optimization method.[17] As shown in,[5] the gradient vector of the quantity of interest can be written as

$$\nabla \mathcal{F}(\beta) = - \left\{ \begin{array}{c} \left[\nabla T \cdot \nabla p\right], \left[\text{atan}(k_2 \, (T - k_3)) \, \nabla T \cdot \nabla p\right], \left[\dfrac{k_1 \, (T - k_3) \, \nabla T \cdot \nabla p}{1 + k_2^2 \, (T - k_3)^2}\right], \\ \left[\dfrac{-k_1 \, k_2 \, \nabla T \cdot \nabla p}{1 + k_2^2 \, (T - k_3)^2}\right], \left[(T - T_a) \cdot p\right], \left[\text{atan}(\omega_2 (T - \omega_3))(T - T_a) p\right], \\ \left[\dfrac{\omega_1 \, (T - \omega_3)(T - T_a) p}{1 + \omega_2^2 (T - \omega_3)^2}\right], \left[\dfrac{-\omega_1 \, \omega_2 (T - T_a) p}{1 + \omega_2^2 (T - \omega_3)^2}\right] \end{array} \right\}^{\mathrm{T}}$$

6. RESULTS AND DISCUSSION

As shown in Fig.1, the T_1 weighted MRI image, the canine is laying supine with legs upward. A stainless steel stylet was used to insert the laser catheter consisting of a 400 mm core diameter with 2 mm fiber tip. The reference scale is provided in units of milli-meter. A cropped thermal image of the heating is overlaid onto the anatomy as an illustration of the heating seen due to the power supplied at the laser. In real-time, MRTI data are acquired with 5 planes of complex image data every 5 seconds.

A calibration study was performed based on measured MRTI data with two discretizations of the geometry, 9,296 and 24,437 degree of freedom (DOF) in geometry with 937 dof and 3,723 DOF for the optimization problem, respectively. This represents a significant amount of saving in computation needed for optimization and hence expedites the real-time solution. The space-time norm over the entire computation process was used as the basis for comparison. The initial pre-calibration value of the objective function is provided as a reference. Results indicate that the calibration problem can be solved with high computation efficiency. The convergence history for calibration and optimization problems shows that twenty function-gradient computations are needed approximately to achieved the preset tolerance compatible to MRTI resolution. Results provide an estimate that the lower bound wall clock time needed for a real-time patient-speci

c calibration computation is 3 minutes (for this particular study); 90 seconds worth of sim- ulation for a function-gradient computation takes 9 seconds, which needs to multiply by twenty objective function-gradient computations needed for convergence.

In Fig. 2(a), a finite element model illustrates the tissue heterogeneity after the calibration in terms of difference of error estimation. In Fig. 2(b), the computed temperature field is overlaid onto the MRI image. Figure 3 demonstrates that the accuracy of controlled temperature profile along the cutting lines shown in Fig. 1(b). The power used in the experiment is 5W with calibration cycle of 60 sec.

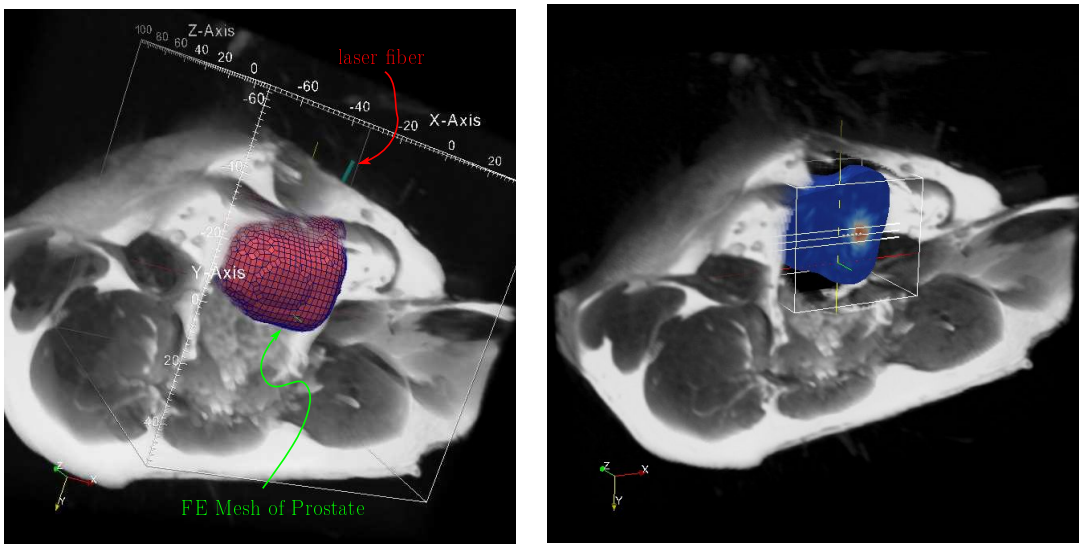

(a) (b)

Figure 1. (a) A finite element model of K9 prostate (b) a thermal image overlaid onto the MRI image.

7. CONCLUSIONS

A computational system for real-time optimal control of laser surgery is presented with biologically relevant quantities formulated in the objective function. We have developed the second generation of the computer code that is more efficient, easy to be parallelized, and capable of accounting for heterogeneity of the computational domain. The *in vivo* experiments on canine indicate that reliable finite element model simulations of LITT can be computed, visualized, and provide predictive control in the same time span that the acutal surgery. Combining these prediction capabilities with an understanding of damage mechanisms at the cellular and tissue

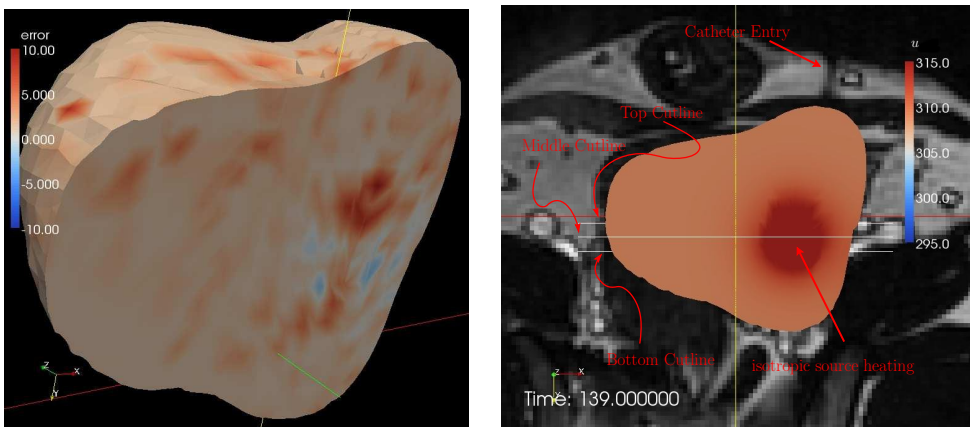

(a) (b)

Figure 2. (a) A finite element domain with heterogeneous tissue properties, and (b) a thermal image overlaid onto the MRI image.

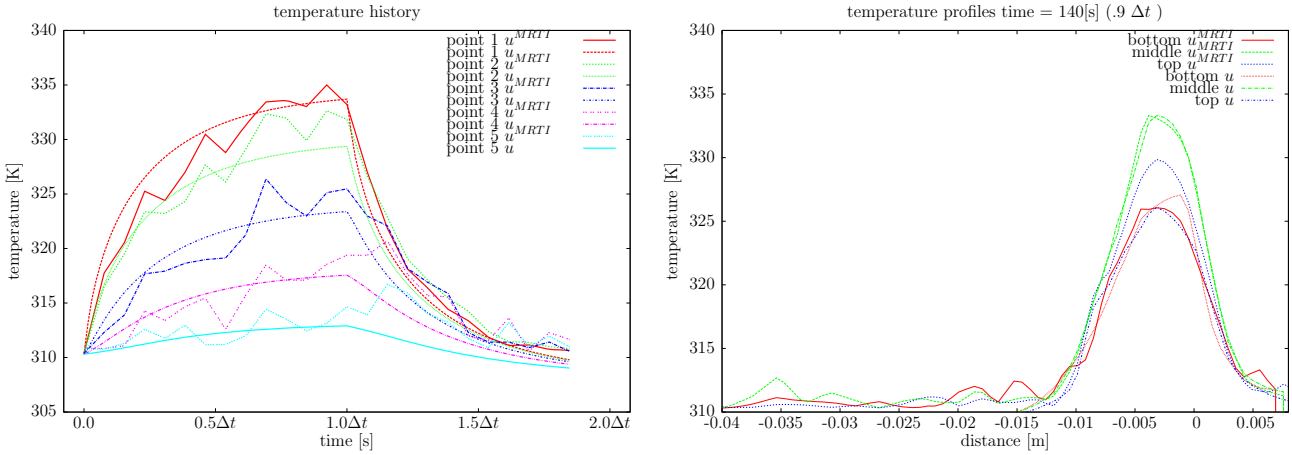

(a) (b)

Figure 3. (a) (a) Temperature profiles for computed and MRTI temperature at the cross points shown in Fig. 1(b) and (b) temperature profiles for the computed and MRTI temperature at the bottom, middle and top cutting lines. The locations of the probe and time history probes are coplanar with the laser tip. The units of time are provided with respect to the time duration of the 5W calibration pulse = 60 sec.

levels under thermotherapeutic conditions can be used as en effective tool for planning and optimizing LITT for cancer treatments. It will provide very powerful tools for surgeons with unprecedented precision and reliability

ACKNOWLEDGMENTS

The research in this paper was supported in part by NIH funding of K25CA116291 (YF) and T32 mechanism (DF). We also would like to acknowledge our collaborators in the first generation of the computational system that we developed in the past three years: Dr. Ivo Babuska, Dr. Jon Bass, Dr. Leszek Demkowicz, Andrea Hawkins, Dr. Chandra Bajaj, Dr. James C. Browne, Dr. Ken Diller from the University of Texas at Austin, as well as Dr. Andrew Elliott, and Dr. John Hazle from M. D. Anderson Cancer Center. The original team members also include Dr. M. Nichole Rylander (currently at Virginia Tech) and Dr. Jessica Zhang (currently at Carnegie-Mellon University). This interdisciplinary team includes experts from mathematics, imaging physics, computer science and visualization, computational science and numerical simulation, and biomedical engineering.

REFERENCES

[1] Kangasniemi et al., M., "Dynamic gadolinium uptake in thermally treated canine brain tissue and experimental cerebral tumors," *Invest. Radiol.* **38**(2), 102–107 (2003).

[2] Salomir et al., R., "Hyperthermia by MR-guided focused ultrasound: accurate temperature control based on fast MRI and a physical model of local energy deposition and heat conduction," *Magn. Reson. Med.* **43**(3), 342–347 (2000).

[3] Vimeux et al., F. C., "Real-time control of focused ultrasound heating based on rapid MR thermometry," *Invest. Radiol.* **34**(3), 190–193 (1999).

[4] Feng, Y., Rylander, M. N., Bass, J., Oden, J. T., and Diller, K., "Optimal design of laser surgery for cancer treatment through nanoparticle-mediated hyperthermia therapy," in [*NSTI-Nanotech 2005*], **1**, 39–42 (2005).

[5] Oden, J., Diller, K., Bajaj, C., Browne, J., Hazle, J., Babuska, I., Bass, J., Demkowicz, L., Feng, Y., Fuentes, D., et al., "Dynamic data-driven finite element models for laser treatment of prostate cancer," *Num. Meth. PDE* **23**(4), 904–922 (2007).

[6] Torres, J., Motamedi, M., Pearce, J., and Welch, A., "Experimental evaluation of mathematical models for predicting the thermal response of tissue to laser irradiation," *APPLIED OPTICS* **32**(4/1) (1993).

[7] Welch, A. and van Gemert, M., [*Optical-thermal Response of Laser-irradiated Tissue*], Plenum Pub Corp (1995).

[8] Niemz, M. and van Gemert, M., [*Laser-tissue interactions: fundamentals and applications*], Springer (2004).

[9] Rylander, M. N., Feng, Y., Bass, J., and Diller, K. R., "Thermally Induced Injury and Heat-Shock Protein Expression in Cells and Tissues," *Annals of the New York Academy of Sciences* **1066**(1), 222–242 (2005).

[10] Pennes, H. H., "Analysis of tissue and arterial blood temperatures in the resting forearm," *J. Appl. Physiol.* **1**, 93–122 (1948).

[11] Rylander, M. N., Feng, Y., and Diller, K. R., "Thermally induced HSP 27, 60, and 70 expression kinetics and cell viability in normal and cancerous prostate cells," *Cell Stress Chaperones* **In review** (2006).

[12] Rylander, M. N., Feng, Y., Zhang, J., Bass, J., J., S. R., Hazle, J., and Diller, K., "Optimizing hsp expression in prostate cancer laser therapy through predictive computational models," *J. Biomed Optics* **11:4**, 041113 (2006).

[13] He, X. and Bischof, J., "Quantification of temperature and injury response in thermal therapy and cryosurgery," *Critical Reviews in Biomedical Engineering* **31**(5-6), 355–421 (2003).

[14] Wright, N., "On a Relationship Between the Arrhenius Parameters from Thermal Damage Studies," *Journal of Biomechanical Engineering* **125**, 300 (2003).

[15] Feng, Y., Oden, J. T., and Rylander, M. N., "A two-state cell damage model under hyperthermic conditions: theory and in vitro experiments ," *Journal of Biomechanical Engineering* **130**(041016), 1–10 (2008).

[16] Feng, Y., Fuentes, D., Hawkins, A., Bass, J., Rylander, M., Elliott, A., Shetty, A., Stafford, R., and Oden, J., "Nanoshell-mediated laser surgery simulation for prostate cancer treatment," *Engineering with Computers* **25**, 3–13 (2009).

[17] Benson, S. J., McInnes, L. C., Moré, J., and Sarich, J., "TAO user manual (revision 1.8)," Tech. Rep. ANL/MCS-TM-242, Mathematics and Computer Science Division, Argonne National Laboratory (2005). http://www.mcs.anl.gov/tao.